THE GEOLOGICAL SOCIETY OF AMERICA®

Monitoring Spatial-Temporal Change of Land Desertification in a Fragile Sub-Alpine Rangeland Eco-Environment: A Case Study from China

WEI XIAN[1]

College of Resources and Environment, Chengdu University of Information Technology, No. 24, Section 1, Xue Fu Road, the Southeast Airport Economic Development Zone, Chengdu, Sichuan Province 610225, China

ZHIYING XIANG

LIYANG LIU

HUAIYONG SHAO

Key Laboratory of Geoscience Spatial Information Technology, Ministry of Land and Resources of the P. R. China, Chengdu 610059, China

Key Terms: ***Land Desertification, Zoige County, Spectral Mixture Analysis, Change Vector Analysis, Ecological Suggestions***

ABSTRACT

Zoige County, China, represents a fragile sub-alpine rangeland eco-environment with a severe land desertification problem. This paper aims at detecting land desertification change in Zoige County over 15 years with quantitative remote-sensing techniques using multi-spectral imagery. Landsat images acquired in 1994 and 2009 were analyzed using the following methodology: (1) image pre-processing; (2) spectral mixture analysis (SMA) to obtain precise sub-pixel classification results of land cover; and (3) change vector analysis (CVA) to conduct a multi-temporal comparison process. Change detection results depict the land desertification conditions and vegetation re-growth conditions. In this way, we characterized the spatial-temporal change pattern of land desertification in Zoige County between 1994 and 2009. After categorizing ecological regions based on change detection results, we analyzed the driving factors of both land desertification conditions and vegetation re-growth conditions, finding out that grasslands under intense grazing pressure tend to suffer severe desertification, while topographic relief has an obvious influence on vegetation re-growth. Specific suggestions for each ecological region are proposed, which can assist the development of environmental restoration measures and environmental protection measures in Zoige County in an effective way. Furthermore, this methodology for monitoring land desertification could be carried out across neighboring counties or in other regions with similar sub-alpine rangeland and land desertification problems.

INTRODUCTION

China is one of the many countries around the globe facing a serious problem of land desertification (Heshmati and Squires, 2013). Land desertification areas in China cover 2.632 million km^2, accounting for 27.33 percent of its total national territory (SFA, 2011). Due to its wide distribution, land desertification threatens the living conditions of nearly 200 million people in China (DPSSTS, 2002). Land desertification affects a wide range of benefits provided by the environment to humans: products such as food and water, natural processes such as climate regulation, and also non-material services such as recreation, and supporting services such as soil conservation (Millennium Environment Assessment, 2005). Moreover, land desertification has environmental impacts that go beyond the areas directly affected. For instance, wind erosion of the desertified areas can increase the formation of large dust clouds that can cause health problems in more densely populated areas thousands of kilometers away (Wang, 2004). To combat desertification, large-scale and long-term monitoring is needed to understand desertification processes and determine the extent of land desertification. Remote-sensing techniques stand out as a time- and cost-efficient method for monitoring

[1]Corresponding author email: xianwei@cuit.edu.cn.

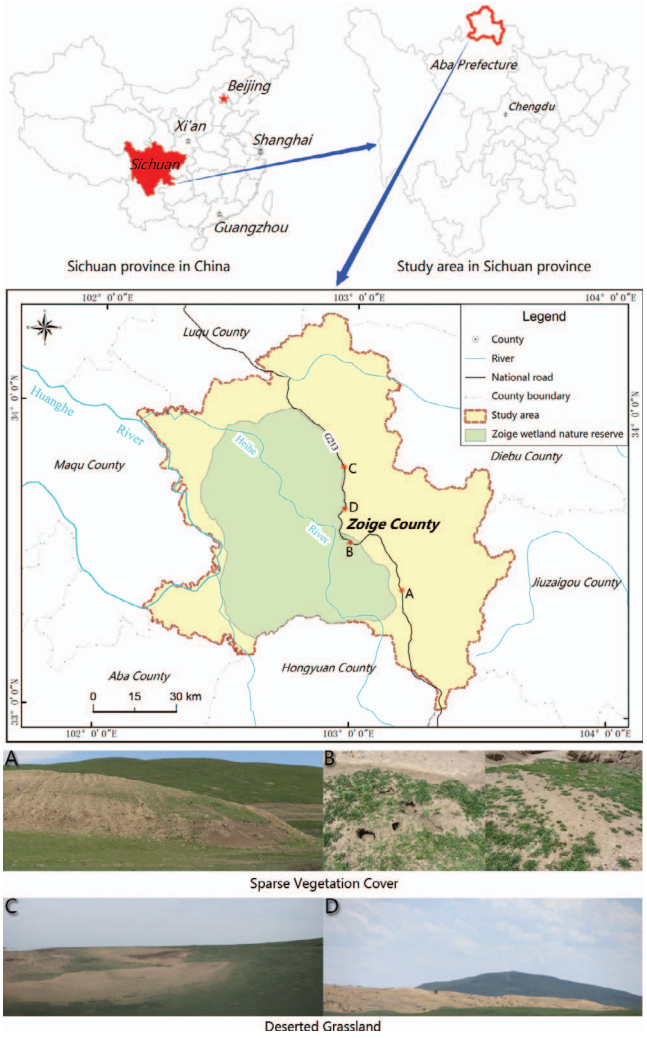

Figure 1. Location of Zoige County and field photos (A, B, C, D indicate the locations of field photos).

land desertification (Helldén, 1984; Tripathy et al., 1996; and Collado et al., 2002).

Using remote-sensing techniques, previous research has mostly focused on desertification in arid and semi-arid areas. Commonly applied approaches to detecting land desertification are vegetation indices such as the NDVI (Normalized Difference Vegetation Index) (Piao et al., 2005; Huang and Siegert, 2006) which is calculated from visible and near-infrared bands and image classification (Wu and Ci, 2002; Qi et al., 2012). However, land desertification of sub-humid and humid areas in China is still lacking research (Wang, 2004). Zoige County, through which the upper Yellow River flows, is located on the northeastern part of Qinghai-Tibet Plateau, with a typical humid plateau climate in a frigid temperate zone. Under the influence of climate change and stock over-grazing, land desertification has been a severe environmental problem in Zoige County since the early 1990s, threatening its fragile sub-alpine rangeland eco-environment and its water conservation functions (Dong et al., 2010).

In the remote-sensing images of Zoige County where grassland, wetland, and sandy soil are distributed closely, one pixel usually contains mixed spectral information due to the high variability in the distribution of land-cover components. According to a previous case study in Zoige (Qiu et al., 2009), supervised classification, which has been commonly used for monitoring land desertification, is sensitive to pixel-level changes of land-cover components. Therefore, this paper applies a sub-pixel classification technique, spectral mixture analysis (SMA), to improve accuracy of land desertification monitoring in Zoige. SMA is designed to derive the proportions of vegetation, sandy soil, and water that compose a mixed pixel to monitor land desertification in a precise way. SMA has been proven effective in a variety of quantitative applications with multi-spectral imagery (Peddle et al., 1999; Small, 2001; Okin et al., 2004; Powell et al., 2007). Therefore, applying SMA to monitor land desertification in a fragile sub-alpine rangeland eco-environment with humid plateau climate has much potential.

MATERIALS AND METHODS

Study Area

Zoige County (seen in Figure 1), which is located on the northeastern part of the Qinghai-Tibet Plateau, covers 10,436.58 km^2 (latitude 32°56′–34°19′N, longitude 102°08′E–103°39′E). Plateau hills and alpine valleys form its landscape. Containing the headwaters of the Yellow River, Zoige County has a crucial water conservation function for southwest China. It enjoys a humid plateau climate in a frigid temperate zone with annual rainfall ranging from 600 to 750 mm. Average annual temperature is around 1°C, with the lowest −10.3°C in January and the highest 10.9°C in July. The major vegetation types in Zoige County are sub-alpine meadow and marsh-meadow, dominated by *Festuca nivina*, *Kobresia setchuanensis*, *Elymus nutans*, *Carex muliensis*, and *Kobresia tibetica*; soil types in Zoige County include peat moor soil, alpine meadow soil, sub-alpine meadow soil, swamp soil, and swampy meadow soil (Yong et al., 2003). Grassland accounts for more than 60 percent of the total land cover area in Zoige County; therefore, pastoral farming has been a major part of local husbandry for centuries. Wetland is distributed widely in Zoige County: 178 plant and 218 animal species have been identified in the Zoige National Wetland Nature Reserve. Among them,

about one third of birds (46 species) and 40 percent of mammals (10 species) belong to international or national protected birds and animals (McNamee, 2003). With the impacts of global climate change and stock over-grazing, land desertification has been a severe environmental problem in this area for decades.

Data Acquisition and Pre-Processing

Landsat-5 Thematic Mapper (TM) images of the studied area on the dates of August 4, 1994, and July 28, 2009, were acquired. For each date, acquired images were on the tracks of path130/row37, path131/row36, and path131/row37, respectively. Multi-temporal images were analyzed to monitor spatial-temporal change of land desertification in Zoige County in the 15 year period. Landsat-5 TM has a spatial resolution of 30 m with six visible/near infrared bands and one thermal band. Bands 1 (0.45–0.52 μm), 2 (0.52–0.60 μm), 3 (0.63–0.69 μm), 4 (0.76–0.90 μm), 5 (1.55–1.75 μm), and 7 (2.08–2.35 μm) from the Landsat-5 TM sensor for both dates were used for the analysis. Band 6 (10.4–12.5 μm) was not included in the analysis because the thermal infrared wavelengths are not required for performing atmospheric correction.

For the application of SMA, conversion from digital values to reflectance was carried out by atmospheric correction for all TM images. The atmospheric correction is based on a revision of the dark-object method, which estimates atmospheric transmissivity as a function of the cosine of the zenith angle (Chavez, 1996). Reflectance for the six non-thermal channels is then computed as follows:

$$\rho_k = \frac{K\pi(L_{sen,k} - L_{a,k})}{E_{0,k}(\cos\theta_i)^2} \quad (1)$$

where ρ_k is the reflectance for band k, K is a factor that takes into account the variation of the Sun-Earth distance; $L_{sen,k}$ is the radiance detected by the sensor (computed from the digital values using the calibration coefficients included in the image); $L_{a,k}$ is the atmospheric radiance, computed from the minimum (dark-object) value of that band; and $E_{0,k}$ is the solar irradiance at the top of the atmosphere and the solar zenith angle. K is computed as a function of the Julian day (D):

$$K = 1 + 0.0167(sen(2\pi(D - 93.5)/365)) \quad (2)$$

It can be seen from the formula above that the dark-object method does not consider the situations of atmospheric multiple scattering or multiple scattering between objects. In addition, the dark-object method does not consider topographic influences. Therefore, the results of dark-object atmospheric correction can be affected by these facts.

Geometric precision correction was applied to all TM images. Each TM image was geo-registered to an existing geo-referenced image using nearest-neighbor re-sampling with 20 control points, and an average root mean square (RMS) error of 0.5 was calculated, which was appropriate for multi-temporal comparisons. In addition, the Shuttle Radar Topography Mission (SRTM) 90 m digital elevation model (DEM) on the track of column 56/row 6 was also acquired for the purpose of topographic analysis in the study area.

Spectral Mixture Analysis

SMA is a technique to derive sub-pixel cover fractions of surface materials using high-spectral-resolution reflectance measurements collected from airborne or space-borne spectrometers (Asner et al., 2003). This method is ideal for use in a sub-alpine, sub-humid rangeland eco-environments where sub-pixel cover variation is high. The goal of SMA is to identify primary spectral contributions within each pixel (Adams et al., 1993). It provides a means to determine the relative abundance of land-cover materials present in any pixel based on the spectral characteristics of the materials.

SMA transforms radiation or reflectance data into fractions of a few dominant end members, which are fundamental physical components of the scene and not themselves a mixture of other components (Elmore et al., 2000). Each end-member component contributes to the pixel-level spectral reflectance, expressed as:

$$R_i = \sum_{j=1}^{n} F_j \cdot RE_{ij} + \varepsilon_i \text{ and } \sum_{j=1}^{n} F_j = 1 \quad (3)$$

$$\text{RMS} = \sqrt{\sum_{i=1}^{B} \frac{(\varepsilon_i)^2}{B}} \quad (4)$$

where R_i is the reflectance of the mixed spectrum in band i, F_j is the fractional abundance of end-member j, RE_{ij} is the reflectance of the end-member spectrum j in band i, n is the number of spectral end members, and ε_i is the error of the fit for band i. Thus, for this analysis with TM data, there will be six equations, one for each spectral band ($B = 6$). Equation 4 is the total root-mean square error (RMSE), where B is the total number of spectral bands.

End-Member Selection

The crucial step to a successful SMA is the selection of appropriate end members. End-member selection techniques, which directly impact modeling performance, vary depending on the tradeoffs among classification accuracy, library size, and computation time (Roth et al., 2012). End members must define a coherent set of spectra that are representative of physical components on the surface, but they must also model the spectral variability inherent to the scene (Elmore et al., 2000). End members can be identified using (1) libraries of known spectra collected with a spectrometer in the field or in a laboratory, (2) libraries of known spectra from previous SMA studies, or (3) spectrally pure or ''extreme'' pixels identified within the images being analyzed (Schweik and Green, 1999). Although image end members cannot be entirely pure, their degree of pureness is more accurate because they represent the dimensionality of the corresponding data set. Thus, they are more suitable for multi-temporal change detection. Aiming at monitoring land desertification, this paper applies image endmembers that were derived with three steps: (1) spectral reduction by the minimum noise fraction (MNF) transform, (2) spatial reduction with the pixel purity index (PPI) method, and (3) manual identification of the end members using the N-dimensional visualizer. The MNF transform, which consists of two consecutive data reduction operations, aims to ensure valid dimensions of imagery data by separating noise from it, thereby reducing the calculation amount of later procedures (Green et al., 1988). The PPI, which has been widely used in multi-spectral and hyper-spectral images analysis for end-member extraction, aims to search for a set of vertices of a convex geometry in a given data set that are supposed to represent pure signatures present in the data (Chaudhry et al., 2006). The N-dimensional visualizer is an interactive tool; by adding in PPI results (relatively pure pixels), it can interactively assist researchers to select image end members in N-dimensional space. In this case study, five image end members were manually selected: bright vegetation (BV), bright soil (BS), dark vegetation (DV), dark soil (DS), and water. The fractions of soil and vegetation can facilitate the analysis of land desertification and vegetation re-growth in the studied area.

Change Vector Analysis

CVA is a radiometric technique that examines the corresponding pixels of two satellite images by comparing two bands of each image to produce images of change magnitude and change direction (Kuzera et al., 2005). In this study, bright vegetation (BV) and bright soil (BS) fraction images were used to monitor the land desertification and vegetation re-growth between 1994 and 2009. The change magnitude of the vector is calculated from the Euclidean distance. The results show the difference between the pixel values of the fraction images for bright vegetation (BV) and bright soil (BS) cover, respectively, between 1994 and 2009. It is shown as follows:

$$R = \sqrt{(\mathrm{BS}_1 - \mathrm{BS}_2)^2 + (\mathrm{BV}_1 - \mathrm{BV}_2)^2} \qquad (5)$$

where R is the magnitude of vector change, and subscripts 1 and 2 indicate the fraction covers in 1994 and 2009.

Change direction is measured as the angle (α) of the change vector from a pixel measurement in 1994 to the corresponding pixel in 2009 according to:

$$\tan\alpha = \frac{(\mathrm{BS}_1 - \mathrm{BS}_2)}{(\mathrm{BV}_1 - \mathrm{BV}_2)} \qquad (6)$$

Angles measured between 90 and 180 degrees indicated an increase in sandy soil and decrease in vegetation cover and therefore represent land desertification conditions. Meanwhile, angles measured between 270 and 360 degrees indicate a decrease in sandy soil and an increase in vegetation cover and therefore represent vegetation re-growth conditions (Lorena et al., 2002). Angles measured between 0 and 90 degrees and between 180 and 270 degrees indicate either an increase or decrease in both sandy soil and vegetation cover, and consequently persistent conditions.

Field Survey

The field survey was conducted in August 2011 in order to evaluate the accuracy of SMA using ground vegetation data as a reference. In total, 30 sampling sites (size 60 $\times$ 60 m for each site, corresponding to four pixels of the Landsat image) were located and established in the study area. At each site, trees and bushes were geo-referenced with a global positioning system (GPS), and then the percentage of ground vegetation cover including sub-alpine meadow, marsh-meadow, and shrubs was estimated using the line-point intercept sampling method. Measurements were taken along 30 60-m-long transects oriented in a N-S direction. Pin flags were lowered at 60 cm intervals along the entire length of the transect. At each point, the types of cover were recorded, and the percentage of vegetation cover was calculated. The accuracy of SMA

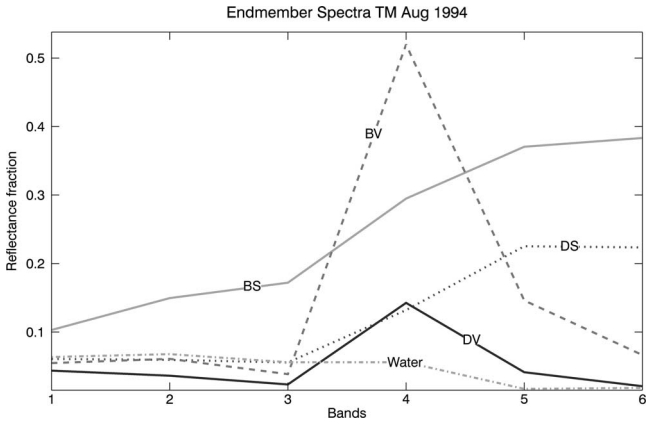

Figure 2. End-member spectra, where BV represents bright vegetation component, DV represents dark vegetation component, BS represents bright soil component, and DS represents dark soil component.

was estimated by scatter plotting correlations of the total percentage of vegetation cover in each plot and the vegetation fraction image.

RESULTS AND DISCUSSIONS

End-Member Spectra

The MNF transform was applied on each TM image to complete spectra reduction. It is found that the first four bands that are generated after transform contain 92 percent of the variance. In the meanwhile, spatial reduction for the MNF transform result was performed with the PPI method. Finally, using the N-dimensional visualizer, five end members were manually selected: bright vegetation (BV), dark vegetation (DV), bright soil (BS), dark soil (DS), and water. BV consists of vegetation with high water content, such as meadow, marsh-meadow, and shrubs. DV consists of vegetation with low water content, such as senescing meadow and senescing shrubs. BS consists of sandy soil with high reflectance and low water content. DS consists of bare soils with low reflectance and high water content. The water end member consists of rivers, lakes, and water areas in wetlands. A set of end-member spectra extracted from one of the August 4, 1994, images is shown in Figure 2.

SMA Process

To achieve the best quality of fraction images, three sets of end members were tested in the SMA process for each TM image. The sets were: (1) all five end members; (2) BV, BS, DS, and water; and (3) BV, BS, and water. Fraction images derived from the different sets of end members were evaluated using visual interpretation, and error extent and distribution in the error fraction image. The set of four end members (BV, BS, DV, and DS) was chosen, since it provided the best distinction of land-cover types and relatively low errors. Proportions of BV, BS, DS, and water for each TM image, presented as fraction images, were determined after the SMA process. The vegetation cover information carried by BV fraction images and the sandy soil cover information carried by BS fraction images separately indicate land desertification (as shown in Figure 3) and vegetation re-growth (as shown in Figure 4). Also, in combination, they contribute to the analysis of wetland degradation in wetland areas (as shown in Figure 5), because detection of an increase of both vegetation cover and soil cover near water implies the degradation of wetland.

The scatter plot correlation between the percentage of vegetation derived from SMA on the TM image (July 2009) and field data (August 2011) is shown in Figure 6. As shown, the R^2 of 0.8942 represents an appropriate correlation between them. In addition, there are possible sources of error that may have affected the correlation result. First of all, the imprecise registration of multi-date images is potentially the largest source of error (Elmore et al., 2000), especially in our case, as the geometric rectification was done with 20 ground control points for each image. In addition, the application of the line-point intercept sampling method in the field survey contains error. Additionally, although the average cloud coverage percentage of images is quite low, cloud shadow in images can possibly affect SMA results lightly. In spite of the existing slight error, the correlation between SMA data and field data in our case shows an acceptable capacity to conduct the multi-date images comparison.

Change Detection

CVA applies BV and BS fraction images to monitor land desertification and vegetation re-growth between 1994 and 2009. The change directions that were derived from CVA indicate both land desertification and vegetation re-growth. The magnitude ranges from low level to high level for both land desertification condition and vegetation re-growth condition (shown in Figure 7). Overall, land desertification prevailed over vegetation re-growth. The land desertification area covers 2,609.66 km^2 in total in Zoige County, including 466.57 km^2 high-level area, 949.36 km^2 medium-level area, and 1,193.73 km^2 low-level area. The high-level areas of land desertification are concentrated in the northwest part of Zoige County. This is caused by long-term integrated driving factors such as climate change and stock over-grazing (Zhang et al., 2007; Shi and Tu, 2009),

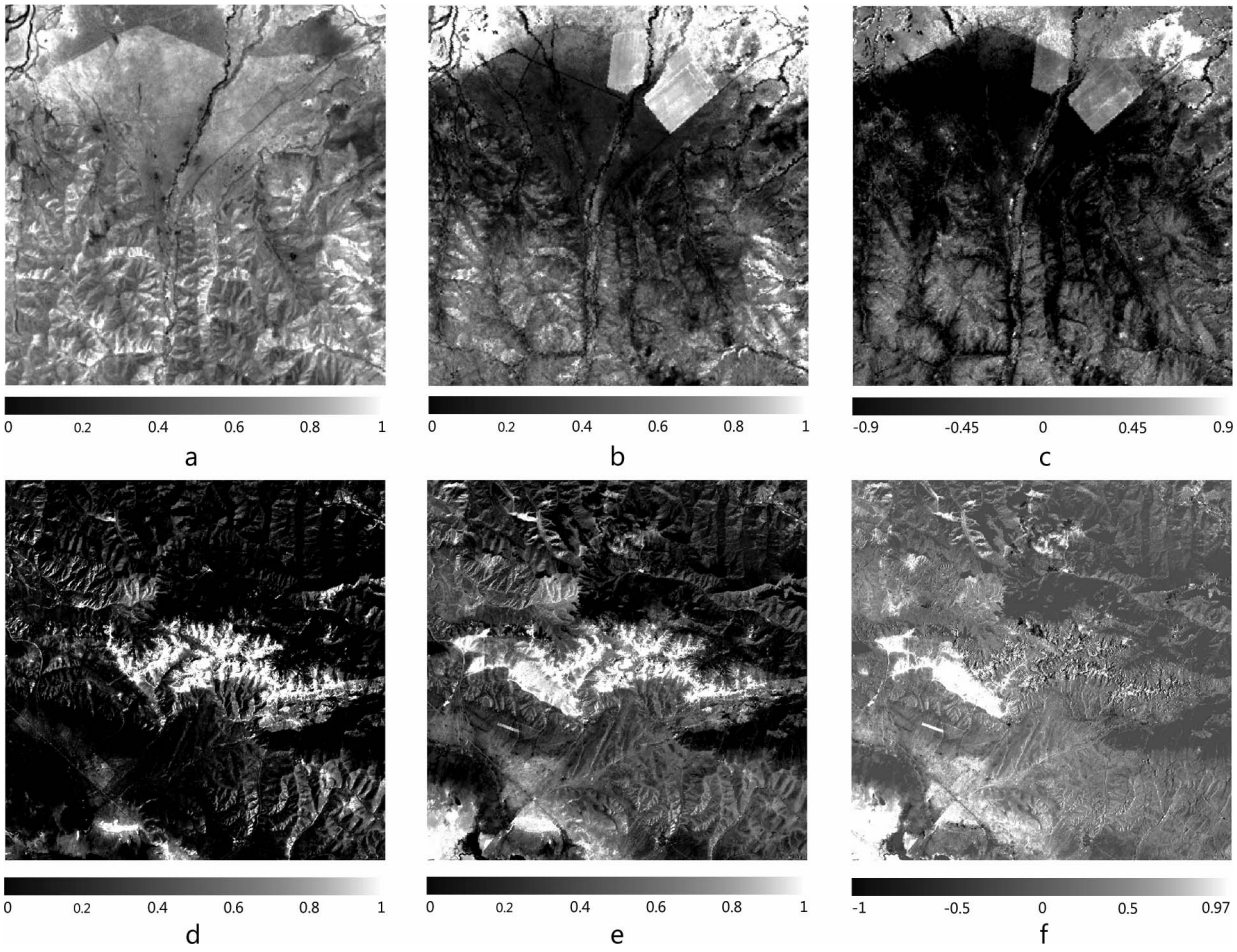

Figure 3. BV and BS fraction images and differences between 15 years: (a) BV in 1994, (b) BV in 2009, (c) difference in BV, (d) BS in 1994, (e) BS in 2009, (f) difference in BS.

threatening the fragile sub-alpine environment in Zoige County. The medium-level areas of land desertification are distributed near high-level areas as transition zones to low-level areas of land desertification. Meanwhile, the vegetation re-growth areas cover 2,383.90 km^2 in total, which consists of 299.33 km^2 high-level areas, 917.09 km^2 medium-level areas, and 1,167.48 km^2 low-level areas. Medium-level

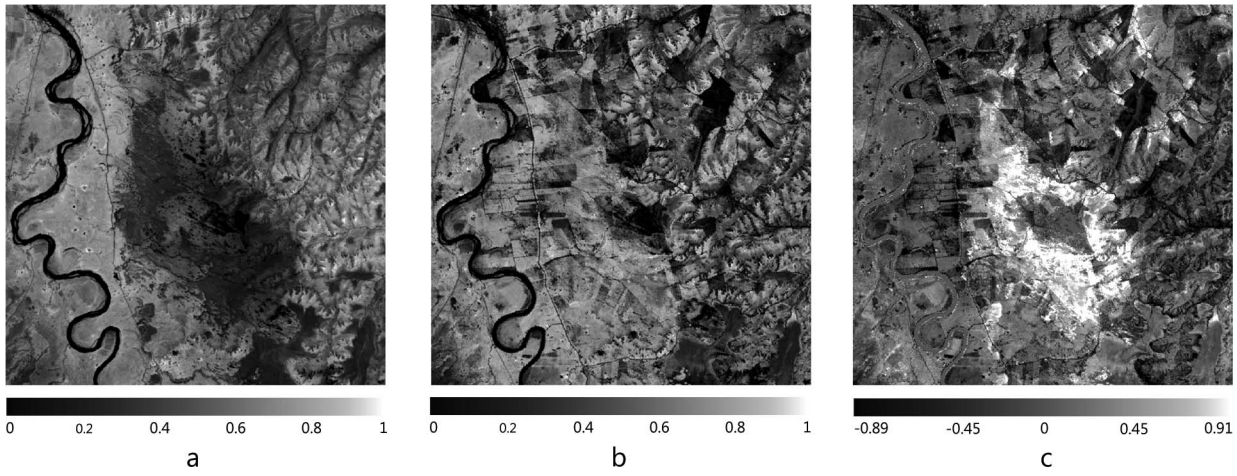

Figure 4. BV fraction images and differences between 15 years: (a) BV in 1994, (b) BV in 2009, (c) difference in BV.

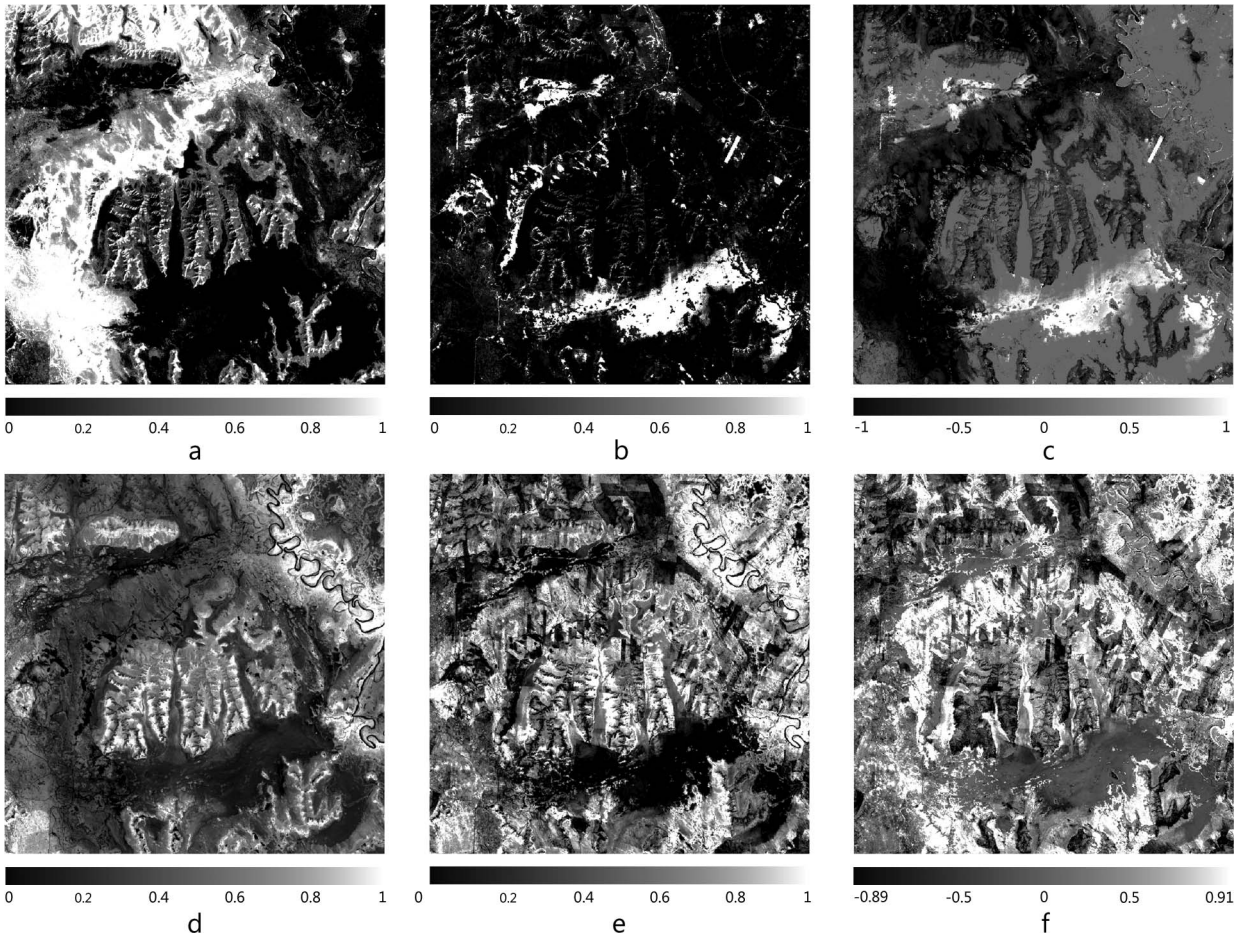

Figure 5. BV and BS fraction images and differences between 15 years: (a) BS in 1994, (b) BS in 2009, (c) difference in BS, (d) BV in 1994, (e) BV in 2009, (f) difference in BV.

and low-level vegetation re-growth conditions were detected mainly in the southeast and northeast of study area where alpine valleys are distributed. A high level of vegetation re-growth conditions was detected in national ranches located in the western part of Zoige County, where land desertification combating measures have been carried out for years.

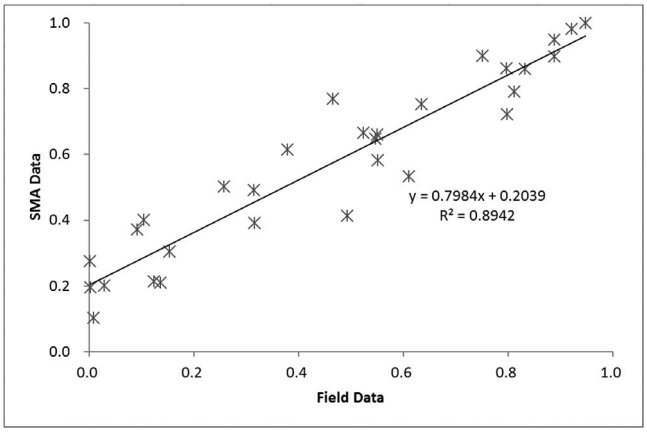

Figure 6. Scatter plot correlation between measured and SMA estimated vegetation fraction in 2009.

ECOLOGICAL SUGGESTIONS

Categorizing Ecological Regions Based on CVA Result

For a further understanding of the spatial-temporal change of land desertification in Zoige County between 1994 and 2009, a more specific and visualized classification for land desertification conditions and vegetation re-growth conditions is needed. Considering the concentrated distribution of similar levels for both land desertification conditions and vegetation re-growth conditions, we categorized Zoige County into three regions (shown in the left part of Figure 8). Respectively, region I represents concentrated areas of land desertification conditions, region II represents concentrated areas of vegetation re-growth conditions, and region III represents concentrated areas of persistent conditions.

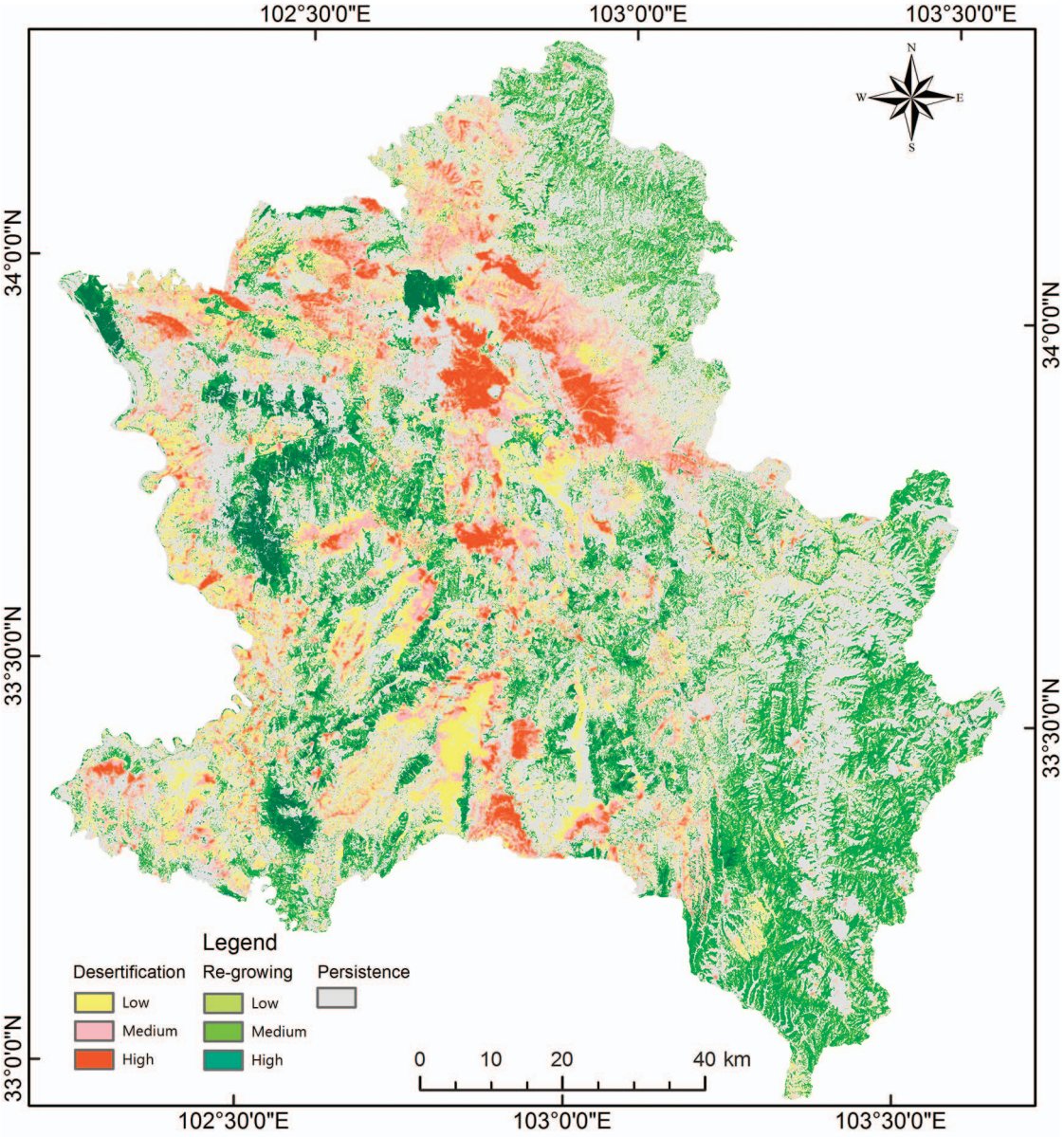

Statistical Table

Desertdication

low		medium		high		sum	
km^2	%	km^2	%	km^2	%	km^2	%
1193.73	45.74	949.36	36.38	466.57	17.88	2609.66	100.00

Re-growing

low		medium		high		sum	
km^2	%	km^2	%	km^2	%	km^2	%
1167.48	48.97	917.09	38.47	299.33	12.56	2383.9	100.00

Figure 7. Distribution map and statistical table of land desertification and vegetation re-growth areas by applying change vector analysis.

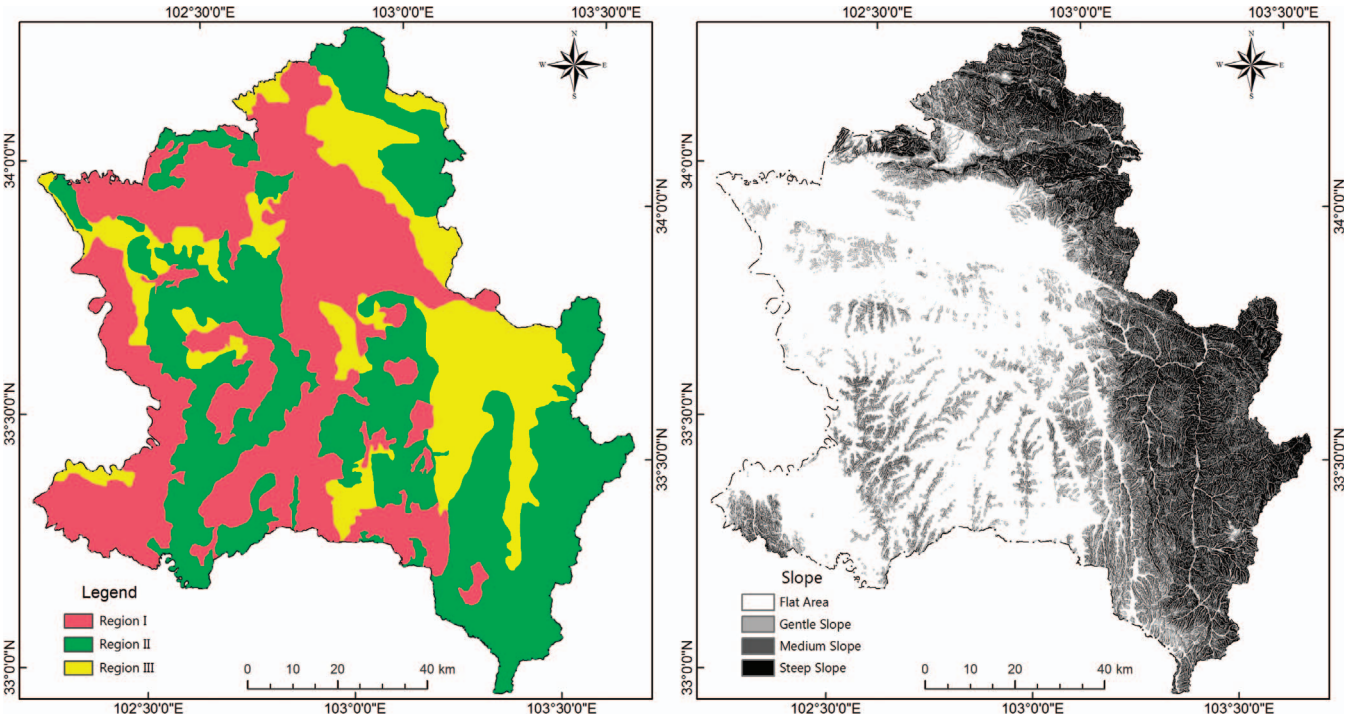

Figure 8. Concentration areas of land desertification, vegetation re-growth, and persistence, categorized according to the change results between 1994 and 2009 in Zoige County (on the left). Slope distribution map of Zoige County (on the right).

Analysis of Driving Factors

Driving Factors of Land Desertification

Climate Change—Under the influence of global climate change, the average annual temperature in Zoige County has been rising significantly for decades at an average rate of 0.28°C/10 yr (Zhang et al., 2007), which is faster than the average rate of global temperature rising 0.03–0.06°C/10 yr (Houghton et al., 2001). Meanwhile, the average annual precipitation in Zoige County has been declining with an average rate of −11.559 mm/10 yr; the average annual evaporation in Zoige County has been increasing with an average rate of 7.621 mm/10 yr (Guo and Li, 2007). As a result of the long-term effects of temperature rises, precipitation declines, and evaporation increases, Zoige County has been suffering from strong winds and droughts in winter and spring (Shi and Tu, 2009). Therefore, there has been a decrease of both the ground vegetation cover (Wang and Zhao, 2005) and the organic matter content of surface soil (Zhao and He, 2000).

Stock Over-Grazing—Pastoral farming is the pillar industry of Zoige County, contributing more than 90 percent of local husbandry income (Jiang and Li, 2012). The ideal maximum of stock capacity in Zoige County is 1.865×10^6 sheep (Shen and Wang, 2003); however, according to the provincial survey of rangeland resources, the actual stock capacity in Zoige County had already reached up to 3.412×10^6 sheep by the end of 2006, overloading the capacity by about 80.1 percent. The overloaded stock capacity in Zoige County leads to stock over-grazing. Long-term stock over-grazing in Zoige County badly affects the growth of vegetation, causing a decrease of grassland productivity and ecological resilience; over-trampling upon grassland by large amounts of stock causes soil hardening and vegetation decrease in Zoige County (Wang and Bao, 2002).

Driving Factors of Vegetation Re-Growth

Protection Measures of National Wetland Nature Reserve—Approved by the State Council, Zoige National Wetland Nature Reserve was established in 1998 (Wang, 2012). Since then, protection measures towards land desertification, such as vegetation restoration and fencing protection, have been effectively carried out within and beyond the boundaries of National Wetland Nature Reserve in Zoige County. In this paper, CVA results shows a fine vegetation re-growth condition around the National Wetland Nature Reserve, which confirms that the protective measures towards land desertification have improved the ground vegetation cover percentage a lot.

Topographic Influences—After analyzing SRTM 90 m DEM data, it is clear that grassland and wetland dominate the land-cover types in Zoige County, while southeastern and northeastern Zoige County contains large areas of alpine valley with an altitude ranging from 2,400 m to 4,200 m. In addition, a slope distribution map of Zoige County (shown in the right part of Figure 8) was generated from DEM data, classified into four types: flat area (0 to 7 degrees), gentle slope (7 to 15 degrees), medium slope (15 to 25 degrees), and steep slope (>25 degrees). Due to the precipitous topography, the alpine valley areas in Zoige County, which are dominated by medium and steep slopes, are spared from heavy human use. Therefore, high forest cover remains there, and fine water conservation function is preserved.

Specific Suggestions for Ecological Regions

Suggestions for Region I (Area of Concentrated Land Desertification Conditions)

Region I, where grassland is widely distributed, has experienced long-term stock over-grazing, which has caused the serious problem of land desertification. Stock capacity control measures such as rotating grazing could alleviate rangeland pressure from stock overloading. At the same time, sparing zones where serious land desertification is caused by livestock grazing and also planting wind-resistant and drought-tolerant species of grasses or shrubs could improve the vegetation cover percentage and rangeland eco-environmental restoration for land desertification areas.

Suggestions for Region II (Area of Concentrated Vegetation Re-Growth Conditions)

Region II, including alpine valley areas and well-restored grassland or wetland areas, presented fine vegetation re-growth conditions. Natural resources protection is necessary for areas with high vegetation cover, especially for alpine forests. Vegetation restoration measures that have proven effective in these areas, such as establishing barriers to protect vegetation during growth period and planting wind-resistant and drought-tolerant vegetation, should be consistently enforced. In this way, it is viable to accomplish the sustainable development of natural resources in region II.

Suggestions for Region III (Area of Concentrated Persistent Conditions)

Region III covers areas where slight land desertification conditions and slight vegetation re-growth conditions have simultaneously been detected, resulting in a relatively persistent condition. For the slight land desertification conditions that are detected in region II, timely and efficient desertification-combating measures should be carried out. For instance, it is recommended to spare zones where land desertification have shown signs because of livestock grazing and to plant appropriate species of grasses until vegetation restoration is completed.

CONCLUSIONS

This paper points out the spatial-temporal change pattern of land desertification in Zoige County by applying SMA and CVA. Between 1994 and 2009, land desertification conditions in Zoige County were concentrated in grassland areas where pastoral farming dominates. Vegetation re-growth conditions were detected in protected areas (National Wetland Reserve and National Ranches) and alpine valley areas, which enjoy fine forest cover. In this study, SMA provided us with precise land-cover information in Zoige County in both 1994 and 2009, which ensures the accuracy of the multi-temporal comparison performance along with the quality of our monitoring results.

After analyzing the driving forces of land desertification in Zoige County, specific suggestions for each ecological region are proposed to help the development of local environment management and efficient measures such as stock capacity control and vegetation restoration to combat land desertification. Combined with long-term remote-sensing monitoring and specific desertification-combating measures, we believe it is possible to restore vegetation cover in land desertification areas in a fragile sub-alpine eco-environment, which will benefit regional eco-environment stability as well as protect land for future generations.

ACKNOWLEDGMENTS

This study is supported and funded by the Key Laboratory of Geoscience Spatial Information Technology, Ministry of Land and Resources of China (Grant No. KLGSIT2013-07), the Research Start-up Funds for Brain Gain of Chengdu University of Information Technology (Grant No. KYTZ201304), the Science & Technology Department of Sichuan Province (Grant No. 2014ZR0145), the National Natural Sciences Foundation of China (Grant No. 41302282), the Research Fund for the Doctoral Program of Higher Education of China (Grant No. 20115122120007), and the National Undergraduate

Training Programs for Innovation (Grant No. 201310616010).

REFERENCES

Adams, J. B.; Smith, M. O.; and Gillespie, A. R., 1993, Imaging spectroscopy: Interpretation based on spectral mixture analysis: *Remote Geochemical Analysis: Elemental and Mineralogical Composition*, Vol. 7, pp. 145–166.

Asner, G. P.; Borghi, C. E.; and Ojeda, R. A., 2003, Desertification in central Argentina: Changes in ecosystem carbon and nitrogen from imaging spectroscopy: *Ecological Applications*, Vol. 13, No. 2, pp. 629–648.

Chaudhry, F.; Wu, C. C.; and Liu, W., 2006, Pixel purity index–based algorithms for endmember extraction from hyperspectral imagery: *Recent Advances in Hyperspectral Signal and Image Processing*, Vol. 37, No. 2, pp. 29–62.

Chavez, P. S., 1996, Image-based atmospheric corrections—Revisited and improved: *Photogrammetric Engineering and Remote Sensing*, Vol. 62, No. 9, pp. 1025–1035.

Collado, A. D.; Chuvieco, E.; and Camarasa, A., 2002, Satellite remote sensing analysis to monitor desertification processes in the crop-rangeland boundary of Argentina: *Journal of Arid Environments*, Vol. 52, No. 1, pp. 121–133.

Department of Population, Social, Science and Technology Statistics, P.R. China (DPSSTS), 2002, *China Population Statistics Yearbook*: China Statistics Press, Beijing (in Chinese).

Dong, Z.; Hu, G.; and Yan, C., 2010, Aeolian desertification and its causes in the Zoige Plateau of China's Qinghai–Tibetan Plateau: *Environmental Earth Sciences*, Vol. 59, No. 8, pp. 1731–1740.

Elmore, A. J.; Mustard, J. F.; and Manning, S. J., 2000, Quantifying vegetation change in semiarid environments: Precision and accuracy of spectral mixture analysis and the normalized difference vegetation index: *Remote Sensing of Environment*, Vol. 73, No. 1, pp. 87–102.

Green, A. A.; Berman, M.; and Switzer, P., 1988, A transformation for ordering multispectral data in terms of image quality with implications for noise removal: *Geoscience and Remote Sensing*, Vol. 26, No. 1, pp. 65–74.

Guo, J. and Li, G., 2007, Climate change in Zoige plateau marsh wetland and its impact on wetland degradation: *Plateau Meteorology*, Vol. 26, No. 2, pp. 422–428 (in Chinese).

Helldén, U., 1984, Drought impact monitoring: A remote sensing study of desertification in Kordofan, Sudan: *Rapporter och Notiser-Lunds Universitets Naturgeografiska Institution*, Vol. 61, pp. 61.

Heshmati, G. A. and Squires, V., 2013, *Combating Desertification in Asia, Africa and the Middle East*: Springer Press, Netherlands, Berlin, Germany.

Houghton, J. T.; Ding, Y.; Griggs, D. J.; and Noguer, M., 2001, *Climate Change 2001: The Scientific Basis*: Cambridge University Press, Cambridge, U.K.

Huang, S. and Siegert, F., 2006, Land cover classification optimized to detect areas at risk of desertification in North China based on SPOT VEGETATION imagery: *Journal of Arid Environments*, Vol. 67, No. 2, pp. 308–327.

Jiang, J. and Li, A., 2012, Change of wetlands in Zoige Country from 1974 to 2007: *Wetland Science*, Vol. 10, No. 3, pp. 318–326 (in Chinese).

Kuzera, K.; Rogan, J.; and Eastman, J. R., 2005, Monitoring vegetation re-growing and deforestation using change vector analysis: Mt. St. Helens study area. Proceedings, *The ASPRS Annual Conference*: Baltimore, MD, pp. 8.

Lorena, R. B.; Santos, J. R.; and Shimabukuro, Y. E., 2002, A change vector analysis technique to monitor land use/land cover in SW Brazilian amazon: Acre state. Proceedings, *PECORA 15-Integrating Remote Sensing at the Global, Regional and Local Scale,* Denver, CO, USA, pp. 8–15.

McNamee, P., 2003, Management plan for Ruoergai National Nature Reserve, report to GEF. In *UNDP-PR/98G32 Wetland Biodiversity Conservation and Sustainable Use in China.*

Millennium Environment Assessment, 2005, *Environments and Human Well-Being*: Island Press, Washington, DC.

Okin, G. S. and Roberts, D. A., 2004, Remote sensing in arid regions: Challenges and opportunities: *Manual of Remote Sensing*, Vol. 4, pp. 111–146.

Peddle, D. R.; Hall, F. G.; and Ledrew, E. F., 1999, Spectral mixture analysis and geometric-optical reflectance modeling of boreal forest biophysical structure: *Remote Sensing of Environment*, Vol. 67, No. 3, pp. 288–297.

Piao, S.; Fang, J.; and Liu, H., 2005, NDVI-indicated decline in desertification in China in the past two decades: *Geophysical Research Letters*, Vol. 32, No. 6, pp. L06402.

Powell, R. L.; Roberts, D. A.; and Dennison, P. E., 2007, Sub-pixel mapping of urban land cover using multiple endmember spectral mixture analysis: *Remote Sensing of Environment*, Vol. 106, No. 2, pp. 253–267.

Qi, Y.; Chang, Q.; and Jia, K., 2012, Temporal-spatial variability of desertification in an agro-pastoral transitional zone of northern Shanxi Province, China: *Catena*, Vol. 88, No. 1, pp. 37–45.

Qiu, P.; Wu, N.; and Luo, P., 2009, Analysis of dynamics and driving factors of wetland landscape in Zoige, eastern Qinghai-Tibetan Plateau: *Journal of Mountain Science*, Vol. 6, No. 1, pp. 42–55 (in Chinese).

Roth, K. L.; Dennison, P. E.; and Roberts, D. A., 2012, Comparing endmember selection techniques for accurate mapping of plant species and land cover using imaging spectrometer data: *Remote Sensing of Environment*, Vol. 127, pp. 139–152.

Schweik, C. M. and Green, G. M., 1999, The use of spectral mixture analysis to study human incentives, actions, and environmental outcomes: *Social Science Computer Review*, Vol. 17, No. 1, pp. 40–63.

Shen, S. and Wang, J., 2003, Principal factors in retrogression of the Zoige plateau marsh wet land: *Acta Geologica Sichuan*, Vol. 23, No. 2, pp. 123–125 (in Chinese).

Shi, C. and Tu, J., 2009, Remote sensing monitory study on land desertification in Ruoergai Plateau of Sichuan Province during 40 years: *Southwest China Journal of Agriculture Sciences*, Vol. 22, No. 6, pp. 1662–1664 (in Chinese).

Small, C., 2001, Estimation of urban vegetation abundance by spectral mixture analysis: *International Journal of Remote Sensing*, Vol. 22, No. 7, pp. 1305–1334.

State Forestry Administration, P.R. China (SFA), 2011, *A Bulletin of Status of Desertification and Sandification in China*: Electronic document, available at http://www.forestry.gov.cn//

Tripathy, G. K.; Ghosh, T. K.; and Shah, S. D., 1996, Monitoring of desertification process in Karnataka state of India using multi-temporal remote sensing and ancillary information using GIS: *International Journal of Remote Sensing*, Vol. 17, No. 12, pp. 2243–2257.

Wang, F., 2012, *Study of Evaluation in Wetland Protection and Restoration Project*: Unpublished Ph.D. Thesis, Chinese Academy of Forestry, Beijing.

Wang, Q. and Bao, W., 2002, Basic types and characters of the western Zoige meadows and their changes in recent decades: *Chinese Journal of Applied & Environmental Biology*, Vol. 8, No. 2, pp. 133–141 (in Chinese).

Wang, T., 2004, Study on sandy desertification in China: Key regions for studying and combating sandy desertification: *Journal of Desert Research*, Vol. 24, pp. 1–9 (in Chinese).

Wang, Y. and Zhao, Z., 2005, Characteristics of the climatic variation in Zoige in the past 45 years and its effects on the eco-environment in the area: *Journal of Geo-mechanics*, Vol. 11, No. 4, pp. 328–332 (in Chinese).

Wu, B. and Ci, L., 2002, Landscape change and desertification development in the Mu Us Sandland, Northern China: *Journal of Arid Environments*, Vol. 50, No. 3, pp. 429–444.

Yong, G.; Shi, C.; and Qiu, P., 2003, Remote sensing monitoring of sand expansion at fragile grassland ecosystem in Ruoergai Plateau, Sichuan, China: *Journal of Mountain Science*, Vol. 21, No. 6, pp. 758–762 (in Chinese).

Zhang, S.; Guo, H.; and Luo, Y., 2007, Assessment on driving force of climate change & livestock grazing capacity to grassland sanding in Ruoergai: *Chinese Journal of Grassland*, Vol. 29, No. 5, pp. 64–71 (in Chinese).

Zhao, K. and He, C., 2000, Influence of human activities on the Mire in Zoige Plateau and countermeasure: *Scientia Geographica Sinica*, Vol. 20, No. 5, pp. 444–449 (in Chinese).